ChemComm

COMMUNICATION

View Article Online
View Journal | View Issue

Cite this: *Chem. Commun.*, 2018, **54**, 13718

Received 22nd August 2018,
Accepted 5th November 2018

DOI: 10.1039/c8cc06810k

rsc.li/chemcomm

A simple lateral flow biosensor for rapid detection of lead(II) ions based on G-quadruplex structure-switching†

Dou Wang,‡[ab] Chenchen Ge,‡[ab] Kongpeng Lv,[ab] Qingshuang Zou,[ab] Quan Liu,[ab] Liping Liu,*[a] Qinhe Yang*[bc] and Shiyun Bao *[a]

A novel lateral flow biosensor for rapid detection of Pb^{2+} was established for the first time based on Pb^{2+}-induced G-quadruplex structure-switching. Semi-quantitative results could be read by reference to a colorimetric card. The whole process only took 15 minutes with a visual detection limit of 25 nM.

Pb^{2+}, a major non-biodegradable environmental pollutant, is highly toxic and hazardous to human health. Trace levels of lead exposure can severely damage the liver, kidney, and central nervous system.[1,2] The United States Environmental Protection Agency set 72 nM as the maximum contamination concentration for Pb^{2+} in drinking water. Over the past decades, spectrometry[3,4] and mass-spectrometry[5,6] were commonly used for Pb^{2+} detection in the laboratory. However, these methods are not applicable in on-site tests for a series of reasons, such as the requirement of tedious pretreatment steps, highly skilled personnel, and expensive apparatus. Therefore, the development of sensitive and easy-to-use methods for Pb^{2+} detection is desirable for environmental protection, as well as disease prevention and treatment.

To date, several functional nucleic acid probes that can specifically bind to Pb^{2+} have been discovered, including the 8–17 DNAzyme[7] and G-rich sequence.[8,9] 8–17 DNAzyme is a Pb^{2+} dependent RNA-cleaving DNAzyme which irreversibly cleaves RNA at the ribo-adenosine (rA) site of the substrate strand with Pb^{2+} as the cofactor.[10] However, since the rA is easily degraded by the RNA enzyme, the detection process should be performed under demanding experimental conditions. Therefore, assays based on this DNAzyme are more suitable for laboratory detection of Pb^{2+} instead of on-site use. G-quadruplexes are high-order structures formed from G-rich oligonucleotides through the stacking of planar G-tetrads.[11] It has been found that Pb^{2+} could induce the conformational change of the G-rich sequence into a G-quadruplex, which can be characterized by several ways, such as fluorescence,[12] colorimetric,[13,14] and electrochemical methods.[15,16] Nevertheless, the signal readout still required laboratory analytical instruments, such as electrochemical or optical detection platforms.

Recently, strip biosensors have received increasing attention because of their short assay time, user-friendly format, and long-term stability.[17] Besides, the strip platform minimizes the requirements for highly qualified personnel and eliminates complex analysis procedures requiring expensive equipment. So far, researchers have successfully developed a variety of strip biosensors for the detection of nucleic acids,[18,19] proteins,[20,21] stem cells,[22] microorganism,[23,24] and small molecules.[25]

Here, we have constructed an easy-to-use and low-cost lateral flow biosensor for the rapid detection of Pb^{2+} based on G-quadruplex structure-switching. As shown in Scheme 1, while the sample mixed with the DNA 1–2 probe is loaded onto the sample pad of the strip biosensor, the mixture begins to

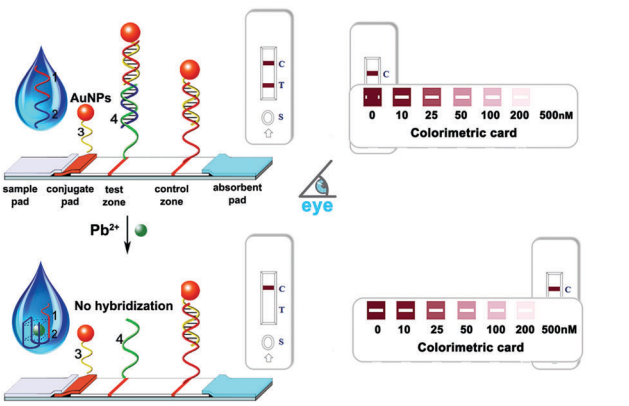

Scheme 1 Schematic illustration of lateral flow biosensor for semi-quantitative visual detection of Pb^{2+} based on Pb^{2+}-induced G-quadruplex formation.

[a] *Department of Hepatobiliary and Pancreatic Surgery, The 2nd Clinical medicine College (Shenzhen People's Hospital) of Jinan University, Shenzhen 518020, China. E-mail: baomi94@163.com*
[b] *Integrated Chinese and Western Medicine Postdoctoral Research Station, Jinan University, Guangzhou 510632, China*
[c] *School of Traditional Chinese Medicine, Jinan University, Guangzhou, 510632, China*

† Electronic supplementary information (ESI) available: Reagents and materials, instruments, experimental procedures and conditions. See DOI: 10.1039/c8cc06810k

‡ Dou wang and Chenchen Ge contributed equally to this work.

migrate by capillary action. If there is no Pb^{2+} in the sample, domain 1 of the DNA 1–2 probe hybridizes with DNA 3 coated on the AuNPs, the AuNP-DNA 3/DNA 1–2 complex continues to migrate along the strip, and is captured by DNA 4 on the test zone through the hybridization with the domain 2 (G-rich sequence, ARGO100).[26] The accumulation of AuNPs at the test zone can form a visible red band. The excess AuNP-DNA 3 conjugates continue to migrate and are captured on the control zone by the hybridization events between DNA 3 and DNA 5, thus forming a second red band. In the excessive presence of Pb^{2+} (for example, 500 nM), DNA 1–2 is assembled into a G-quadruplex which therefore hinders its hybridization with DNA 4. As a result, the red band at the test zone is disappeared. The sequences of DNA 1–2, DNA 3, 4, and 5 are listed in Table S1 (ESI†). To further expand its application, semi-quantitative analysis results can be observed by reference to a colorimetric card, respectively.

At the beginning of the study, the influence of domain 1 (TCGGGTGTGGGTG) on the G-quadruplex formation of domain 2 (GGTGGTGGTGGTTGTGGTGGTGGTGG) was investigated. The conformational change of DNA 1–2 and domains 1 and 2 was examined by CD spectra measurements in the presence of Pb^{2+}. From Fig. 1A, we can see that only DNA 1–2 or domain 2 folded into a parallel G-quadruplex corresponding to a positive ellipticity maximum at 264 nm and a negative maximum at 240 nm.[27] Meanwhile, the positive ellipticity maximum of DNA 1–2 at 264 nm is higher than that of domain 2. These results indicated that although domain 1 is too short to form a G-quadruplex by itself, it can promote and participate in the G-quadruplex formation of domain 2.

The conformational change of the G-rich sequence was simultaneously validated by fluorescence measurements in the presence of Pb^{2+}. Pei's group has reported that *N*-methyl mesoporphyrin IX (NMM) could selectively bind to a G-quadruplex (ARGO100) over single-stranded DNA and double-stranded DNA. The fluorescence signal of NMM is weak in the free state, whereas it is enhanced significantly in the presence of a G-quadruplex.[26] The reason for this phenomenon may be that NMM intercalates and is in close contact with the DNA base pairs of the G-quadruplex, then fluorescence energy transfer from the base pairs to NMM then occurred, resulting in the emission of the fluorescence signal of NMM.[28,29] Therefore, the formation of the G-quadruplex can be characterized by the fluorescence intensity of NMM, and it did not affect the structure of the G-quadruplex (Fig. S1, ESI†). Fig. 1B shows the fluorescence intensity peaks when the ratio of Pb^{2+} to DNA 1–2 concentration reaches 2–3; we speculated that one single-stranded DNA 1–2 and two Pb^{2+} could form a G-quadruplex in the reaction buffer, and the addition of one more Pb^{2+} could form a more compact structure (Fig. 1C). The folding process of Pb^{2+} with DNA 1–2 can be divided into three steps.[30,31] The first step can be interpreted as a Pb^{2+} binding step, which is accompanied by partial folding of DNA 1–2. The second step is presumed to be the folding of DNA 1–2 to give a metastable G-quadruplex, which then rearranges in the third step to give the final folded structure of the G-quadruplex, as shown in eqn (1) below. $(\text{G-rich})_U$ and $(\text{G-rich}\text{–}n\text{Pb}^{2+})_F$ indicate the unfolded and folded structures of the G-rich sequence, respectively. I refers to the intermediate.

$$(\text{G-rich})_U + n\text{Pb}^{2+} \rightleftharpoons \text{I} \rightarrow (\text{G-rich}\text{–}n\text{Pb}^{2+})_F \qquad (1)$$

Nevertheless, the fluorescence intensity gradually decreased with the increase of Pb^{2+} concentration, which may due to the fact that Pb^{2+} is a fluorescence quenching agent[32,33] and a higher concentration of Pb^{2+} could quench the fluorescence of NMM at the binding state (Fig. 1C).

The experimental parameter that affects the sensitivity of the lateral flow biosensor was optimized. The optimization was performed by varying one parameter and keeping constant of other parameters. We found that too high or too low a concentration of DNA 1–2 led to false positive or false negative results. Therefore, the DNA 1–2 concentration was investigated. Fig. S2 (ESI†) depicts the response of $(P_0 - P)$ values to different concentrations of DNA 1–2 from 50 nM to 250 nM. The $(P_0 - P)$ value increased significantly with the DNA 1–2 concentration raised up to 150 nM, and a further increase of the DNA 1–2 concentration induced a remarkable decrease of the $(P_0 - P)$ value. Accordingly, 150 nM was chosen as the optimal concentration of DNA 1–2 in this experiment.

To evaluate the sensitivity and dynamic range of this lateral flow biosensor, different concentrations of Pb^{2+} (0, 10 nM, 25 nM, 50 nM, 100 nM, 200 nM, and 500 nM) were examined under optimal experimental conditions. As shown in Fig. 2A, the color intensity of the red bands on the test zone decreased with the increase of Pb^{2+} concentration. In consideration of the fact that this strip biosensor is a turn-off sensing system for Pb^{2+} detection, one of the most important problems is how to make the test results easy to read. To solve this problem, we provided a colorimetric card corresponding to the red color intensity on the test zone. By using this colorimetric card, the test results could be identified easily and conveniently, which could reduce the error caused by human subjective judgment. When the Pb^{2+} concentration was up to 25 nM, the red color on the test zone was easily distinguishable from 0 nM Pb^{2+} by reference to the colorimetric card. As a result, 25 nM was set as the threshold for the visual determination of Pb^{2+} without

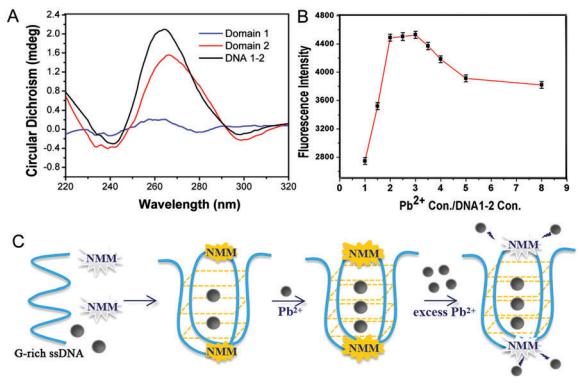

Fig. 1 (A) The influence of domain 1 on the G-quadruplex formation of domain 2 was investigated. (B) The formation of G-quadruplex was validated by fluorescence measurements. (C) The influence of Pb^{2+} concentration on the fluorescence of NMM at the binding state.

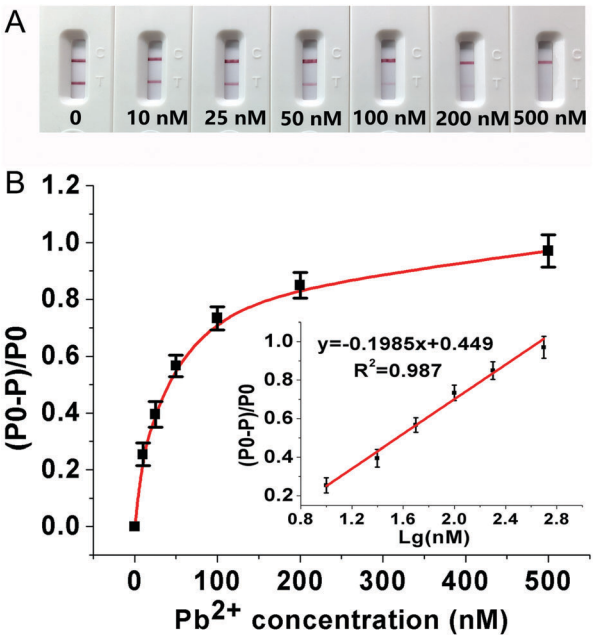

Fig. 2 The sensitivity of this biosensor. (A) Photo images of the strips with different concentrations of Pb^{2+}. (B) Plots of $(P_0 - P)/P_0$ *vs.* Pb^{2+} concentration. Inset: Calibration curve of $(P_0 - P)/P_0$ *vs.* the logarithm of Pb^{2+} concentration. P_0: peak areas of negative samples of the red bands on the test zone, P: peak areas of positive samples of the red bands on the test zone.

instrumentation. The resulting calibration curve suggests that $(P_0 - P)/P_0$ was proportional to the logarithm of Pb^{2+} concentration in the range of 10–500 nM (Fig. 2B). Although the detection limit of this method is higher than those of some reported colorimetric assays, the operation process is simplified and the test time is shortened. A comparison of the detection time and the detection limit for Pb^{2+} is summarized in Table S2 (ESI†).

To validate the specificity of this biosensor, several other competing metal ions, including K^+, Na^+, Cu^{2+}, Hg^{2+}, Mn^{2+}, Mg^{2+}, Fe^{2+}, Zn^{2+}, Cd^{2+}, Sr^{2+}, and Ba^{2+}, were tested as controls. And the mixture of Pb^{2+} (500 nM) with different competing metal ions (each 100 μM, except Cd^{2+}, Sr^{2+}, and Ba^{2+}) was also tested as a control. As shown in Fig. 3A, the red band at the test zone disappeared completely with 500 nM Pb^{2+}, and the coexistence of other metal ions with Pb^{2+} under the test conditions did not apparently affect the Pb^{2+} detection. Their corresponding optical responses were further confirmed by recording the peak areas of the red bands with a strip reader (Fig. 3B). Nevertheless, Cd^{2+}, Sr^{2+}, and Ba^{2+} have moderate interference with the detection of Pb^{2+} due to their ability to stabilize the G-quadruplex structure, and the CD spectra of DNA 1–2 with Cd^{2+}, Sr^{2+} and Ba^{2+} and their corresponding $(P_0 - P)$ values examined by this biosensor are shown in Fig. S3 (ESI†). It is worth noting that when the reaction time was reduced from 10 min to 5 min, the $(P_0 - P)$ values of Cd^{2+}, Sr^{2+}, and Ba^{2+} were apparently suppressed as compared with that of Pb^{2+}. Therefore, the interference from Cd^{2+}, Sr^{2+}, and Ba^{2+} may be reduced by shortening the incubation time for Pb^{2+} detection, and 5 min was selected as the optimum reaction time of this biosensor.

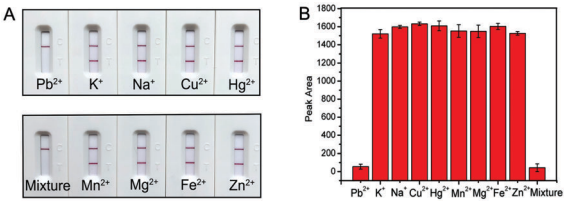

Fig. 3 The specificity of this biosensor. (A) Photo images of the strips with different metal ions. (B) The difference in peak area between Pb^{2+} (500 nM) and other competing metal ions (each 100 μM).

In consideration of the fact that the Na^+ and K^+ concentrations are usually higher than 100 μM in drinking water, and they are also known to induce the formation of G-quadruplexes, the maximum endurance concentrations of Na^+ and K^+ *via* this method were investigated. DNA 1–2 with different concentrations (10 mM, 50 mM, and 100 mM) of Na^+ and K^+ was examined by CD spectrum measurement and the biosensor under optimal experimental conditions, respectively. As shown in Fig. S4A (ESI†), when the concentration of Na^+ is under 50 mM and that of K^+ is under 10 mM, the G-rich sequence presented a random-coil structure, which exhibited two small ellipticities at 240 nm and 264 nm. However, it folded into a parallel G-quadruplex in the presence of 100 mM Na^+ or 50 mM K^+, corresponding to two the characteristic peaks at 264 nm and 240 nm. Meanwhile, the $(P_0 - P)$ value increased significantly in the presence of 100 mM Na^+ and 50 mM K^+ (Fig. S4B, ESI†). Accordingly, the maximum endurance concentration for Na^+ and K^+ of this biosensor is 50 mM and 10 mM, respectively. These results demonstrate that this strip exhibits good selectivity to Pb^{2+} over other competing metal ions.

In summary, a novel strip biosensor for Pb^{2+} detection was designed based on G-quadruplex structure-switching for the first time and the test results could be easily read for semi-quantitative analysis by the use of a colorimetric card. In comparison with previously reported strips for Pb^{2+} detection, this strip biosensor presents a short detection time of only 15 min with an acceptable recovery rate (Table S3, ESI†). Besides, it has other advantages such as simple processing steps, avoidance of any expensive instruments, and the cost of one test is as low as $0.6. Therefore, this strip biosensor equipped with a colorimetric card shows great promise for in-field Pb^{2+} detection. Furthermore, the reagents used for this assay can be lyophilized for portable deployment and storage, which shows great convenience in field testing. Our future work will dive deeper into the specificity issue and combine with optimized sample pretreatment to reduce the interference of competing metal ions using masking agents to make the strip more suitable for field monitoring.

Conflicts of interest

There are no conflicts of interest to declare.

Notes and references

1 M. R. Saidur, A. R. Aziz and W. J. Basirun, *Biosens. Bioelectron.*, 2017, **90**, 125–139.

2 B. Bansod, T. Kumar, R. Thakur, S. Rana and I. Singh, *Biosens. Bioelectron.*, 2017, **94**, 443–455.
3 Y. Jiang and D. Kim, *J. Nanosci. Nanotechnol.*, 2014, **14**, 8578–8583.
4 M. Behbahani, A. Bagheri, M. Taghizadeh, M. Salarian, O. Sadeghi, L. Adlnasab and K. Jalali, *Food Chem.*, 2013, **138**, 2050–2056.
5 E. K. Peterson, D. T. Wilson, B. Possidente, P. McDaniel, E. J. Morley, D. Possidente, K. T. Hollocher, D. M. Ruden and H. V. B. Hirsch, *Chemosphere*, 2017, **181**, 368–375.
6 M. Shamsipur, L. Farzin, M. Amouzadeh Tabrizi and S. Sheibani, *Mater. Sci. Eng., C*, 2017, **77**, 459–469.
7 H. Liu, X. Yu, Y. Chen, J. Zhang, B. Wu, L. Zheng, P. Haruehanroengra, R. Wang, S. Li, J. Lin, J. Li, J. Sheng, Z. Huang, J. Ma and J. Gan, *Nat. Commun.*, 2017, **8**, 2006.
8 Y. Li, C. Wang, Y. Zhu, X. Zhou, Y. Xiang, M. He and S. Zeng, *Biosens. Bioelectron.*, 2017, **89**, 758–763.
9 Y. Zhao, Q. Zhang, W. Wang and Y. Jin, *Biosens. Bioelectron.*, 2013, **43**, 231–236.
10 X. H. Zhao, R. M. Kong, X. B. Zhang, H. M. Meng, W. N. Liu, W. Tan, G. L. Shen and R. Q. Yu, *Anal. Chem.*, 2011, **83**, 5062–5066.
11 Q. Zhu, L. Liu, Y. Xing and X. Zhou, *J. Hazard. Mater.*, 2018, **355**, 50–55.
12 A. Ravikumar, P. Panneerselvam and K. Radhakrishnan, *Mikrochim. Acta*, 2017, **185**, 2.
13 W. Yun, D. Cai, J. Jiang, P. Zhao, Y. Huang and G. Sang, *Biosens. Bioelectron.*, 2016, **80**, 187–193.
14 H. Sun, L. Yu, H. Chen, J. Xiang, X. Zhang, Y. Shi, Q. Yang, A. Guan, Q. Li and Y. Tang, *Talanta*, 2015, **136**, 210–214.
15 L. Wang, Y. Wen, L. Li, X. Yang, N. Jia, W. Li, J. Meng, M. Duan, X. Sun and G. Liu, *Biosens. Bioelectron.*, 2018, **115**, 91–96.
16 F. Gao, C. Gao, S. He, Q. Wang and A. Wu, *Biosens. Bioelectron.*, 2016, **81**, 15–22.
17 J. Chen, X. Zhou and L. Zeng, *Chem. Commun.*, 2013, **49**, 984–986.
18 X. Gao, L. P. Xu, T. Wu, Y. Wen, X. Ma and X. Zhang, *Talanta*, 2016, **146**, 648–654.
19 J. Gomez-Martinez, M. Silvy, J. Chiaroni, C. Fournier-Wirth, F. Roubinet, P. Bailly and J. C. Bres, *Anal. Chem.*, 2018, **90**, 7502–7509.
20 C. Ge, L. Yu, Z. Fang and L. Zeng, *Anal. Chem.*, 2013, **85**, 9343–9349.
21 I. S. Sene, V. C. Silva, G. E. N. Pauli, I. H. Bechtold, L. C. C. Nunes, C. Eiras and C. H. N. Costa, *Recent Pat. Biotechnol.*, 2018, **12**, 221–228.
22 W. Wu, L. Yu, Z. Fang, P. Lie and L. Zeng, *Anal. Biochem.*, 2013, **436**, 160–164.
23 Y. Wang, W. Yan, S. Fu, S. Hu, Y. Wang, J. Xu and C. Ye, *Front. Microbiol.*, 2018, **9**, 907.
24 Y. Xu, Y. Wei, N. Cheng, K. Huang, W. Wang, L. Zhang, W. Xu and Y. Luo, *Anal. Chem.*, 2018, **90**, 708–715.
25 J. Chen, J. Wen, L. Zhuang and S. Zhou, *Nanoscale*, 2016, **8**, 9791–9797.
26 L. Xu, X. Shen, S. Hong, J. Wang, Y. Zhang, H. Wang, J. Zhang and R. Pei, *Chem. Commun.*, 2015, **51**, 8165–8168.
27 C. H. Chung, J. H. Kim, J. Jung and B. H. Chung, *Biosens. Bioelectron.*, 2013, **41**, 827–832.
28 J. B. LePecq and C. Paoletti, *J. Mol. Biol.*, 1967, **27**, 87–106.
29 C. G. Reinhardt, B. P. Roques and J. B. Le Pecq, *Biochem. Biophys. Res. Commun.*, 1982, **104**, 1376–1385.
30 W. Liu, H. Zhu, B. Zheng, S. Cheng, Y. Fu, W. Li, T. C. Lau and H. Liang, *Nucleic Acids Res.*, 2012, **40**, 4229–4236.
31 W. Liu, Y. Fu, B. Zheng, S. Cheng, W. Li, T. C. Lau and H. Liang, *J. Phys. Chem. B*, 2011, **115**, 13051–13056.
32 D. Zhang, M. Zhu, L. Zhao, J. Zhang, K. Wang, D. Qi, Y. Zhou, Y. Bian and J. Jiang, *Inorg. Chem.*, 2017, **56**, 14533–14539.
33 J. Chen, J. Liu, Z. Fang and L. Zeng, *Chem. Commun.*, 2012, **48**, 1057–1059.